IEEE Access
Multidisciplinary | Rapid Review | Open Access Journal

Received 8 October 2023, accepted 5 November 2023, date of publication 9 November 2023, date of current version 17 November 2023.

Digital Object Identifier 10.1109/ACCESS.2023.3331826

RESEARCH ARTICLE

An Intelligent Systemic Circulation Monitoring System for Neonatal Illness Severe Severity Evaluation

HSIU-LIN CHEN[1], BOR-SHING LIN[2], (Senior Member, IEEE), KAI-HUEI CHEN[3], AND BOR-SHYH LIN[3], (Senior Member, IEEE)

[1]Department of Pediatrics, Kaohsiung Medical University Hospital, Kaohsiung 80756, Taiwan
[2]Department of Computer Science and Information Engineering, National Taipei University, New Taipei City 237303, Taiwan
[3]Institute of Imaging and Biomedical Photonics, National Yang Ming Chiao Tung University, Tainan 71150, Taiwan

Corresponding author: Bor-Shyh Lin (borshyhlin@gmail.com)

This work was supported in part by the Ministry of Science and Technology in Taiwan under Grant MOST 110-2221-E-A49-096-MY3; in part by the National Science and Technology Council in Taiwan under Grant NSTC 112-2221-E-305-001-MY3; in part by the Ministry of Health and Welfare in Taiwan under Grant MOHW109-B-212-114006; in part by the Kaohsiung Medical University under Grant NCTUKMU109-BIO-02; in part by the Higher Education Sprout Project of the National Yang Ming Chiao Tung University and the Ministry of Education (MOE), Taiwan; and in part by the Faculty Group Research Funding Sponsorship by National Taipei University under Grant 2023-NTPU-ORD-01.

This work involved human subjects in its research. Approval of all ethical and experimental procedures and protocols was granted by the Institutional Review Board, Kaohsiung Medical University Chung-Ho Memorial Hospital, Taiwan.

ABSTRACT Illness severity is a major determinant of neonatal mortality. In neonatal intensive care, severity-of-illness scales, primarily relied on subjective judgment by experienced physicians, are used to assess the mortality risk prediction and therapeutic intensity. Because cardiovascular morbidity and other disease state may contribute to hemodynamic abnormalities, the illness severity may reflect on the state of hemodynamic abnormalities. Several diagnostic approaches, such as laser Doppler flowmetry and orthogonal polarization spectral, have been developed to evaluate the local information of blood flow or vascular distribution on skin surface, but they may not efficiently evaluate the systemic circulation. In this study, an intelligent systemic circulation monitoring system was proposed to non-invasively evaluate the blood perfusion state and further estimate the illness severity. In the proposed system, a wireless sensing device was designed to real-time monitor the changes of hemoglobin parameters under the altered external pressure, and several indexes were defined from the hemodynamic response to present the blood perfusion state. The relationship between the blood perfusion state and the illness severity was also investigated in this study. Moreover, the technique of neural network was also applied in the classification of illness severity. The experimental results indicate the differences between many defined blood perfusion indexes in neonates with different illness severity were exactly significant and the mild and severe illness severity group could also be efficiently recognized by the neural network technique. Therefore, the proposed system may contain the potential of future clinical applications in the evaluation of illness severity or other diseases.

INDEX TERMS Illness severity, neonatal intensive care, hemodynamic abnormalities, blood perfusion, neural network.

I. INTRODUCTION

The cardiorespiratory system undergoes the structural and functional change from fetal to the postnatal period. Any immature development of organs and organ systems in neonates may cause the irreversible damage and increase the risk of prevalence and mortality. Therefore, it is essential to assist the physician in identifying and predicting for early intervention, especially in the neonatal intensive care unit. Neonatal therapeutic intervention scoring system (NTISS)

The associate editor coordinating the review of this manuscript and approving it for publication was Yizhang Jiang.

© 2023 The Authors. This work is licensed under a Creative Commons Attribution-NonCommercial-NoDerivatives 4.0 License.
For more information, see https://creativecommons.org/licenses/by-nc-nd/4.0/

has been developed to assist physicians for outcome prediction by evaluating the illness severe severity and fatality [1]. However, NTISS is the clinical scales based on interventions and treatments, rather than on the true pathophysiological measurements [2]. Hemodynamic monitoring has been proved to be pivotal for evaluating individualized pathophysiology [3], and therefore, the illness severity may reflect on the hemodynamic state.

In clinical, the capillary refill time (CRT) is the time that it takes for the color changes and regain after pressure is applied to cause skin blanching, and is the widely used examination method to evaluate hemodynamic state and distal capillary perfusion signs [4], [5], [6]. However, in clinical, the estimation of CRT is usually observed subjectively by the medical staffs, and there is still lacks of a monitoring system to objectively evaluate the CRT information. Several methods, such as laser Doppler flowmetry (LDF), magnetic resonance imaging (MRI), and orthogonal polarization spectral (OPS) imaging, may also be applied in the non-invasive microcirculation evaluation. Here, laser Doppler flowmetry can provide the blood flow estimation by measuring the doppler frequency shift resulting from the reflected laser light changes in moving blood cells [7], but it is extremely sensitive to movement artifacts [8]. Based on the differences in the magnetic resonance signal between different human tissue components, the MRI technique can be used to noninvasively assess the hemodynamic changes elicited by blood flow and oxygenation during the hyperemic response, and has been developed in the applications of cerebral blood flow, ventricular function and systemic perfusion in neonates [9]. But the sedation or general anesthesia are commonly required to ensure immobilization during imaging, and this may increase the risk of adverse events, especially for neonates with complex congenital heart disease (CHD) [10]. In the OPS imaging technique, the linearly polarization light is used to illuminate tissue and the cross-polarization of reflected light will enhance the contrast of vascular structures. The microvascular diameter and the red blood cell velocity could be quantified and assessed by the high contrast images of OPS without using florescent dye [11]. Although the above approaches can provide the local information of blood flow or vascular distribution, but they may still not effectively evaluate the systemic hemodynamic. Near-infrared spectroscopy (NIRS) is an optical technique used to non-invasively estimate the change of the human tissue composition, and has been widely developed in the applications of monitoring blood perfusion and tissue oxygenation [12], [13], [14], [15]. We also reviewed the literature review papers [16], [17], [18] on neonatal physiological monitoring. From these literature reviews, it can be seen that most neonatal physiological monitoring is performed using bulky and numerous equipment, and most of them can only monitor a single physiological parameter. There is no system that monitors the systemic circulation and establishes indicators to evaluate the severity of neonatal diseases. Based on the NIRS technique, a novel systemic circulation monitoring system was proposed and implemented in this study, to estimate the blood perfusion information and further evaluate neonatal illness severe severity. Here, a wireless sensing device was designed to real-time and non-invasively monitor the change of the hemoglobin parameters under the applied pressure, and several indexes were also defined to present the blood perfusion state. The relationship between the defined indexes and the illness severity was also investigated in this study. Finally, the neural network technique was used to classify neonates with different illness severe severity.

II. METHODS

A. DESIGN AND IMPLEMENTATION OF SYSTEMIC CIRCULATION MONITORING SYSTEM

The proposed intelligent systemic circulation monitoring system, as shown in Fig. 1, mainly contains a wireless sensing device and a smart platform. The wireless sensing device was designed to acquire and transmit the changes of hemoglobin parameters and the applied pressure under capillary refill test, to the smart platform wirelessly. The smart platform was designed to estimate the blood perfusion state of the newborn baby and further evaluate the illness severity. Here, several defined blood perfusion indexes would be extracted from the change of these hemoglobin parameters, and then would be inputted into the model of neural network to evaluate the state of neonatal illness severe severity.

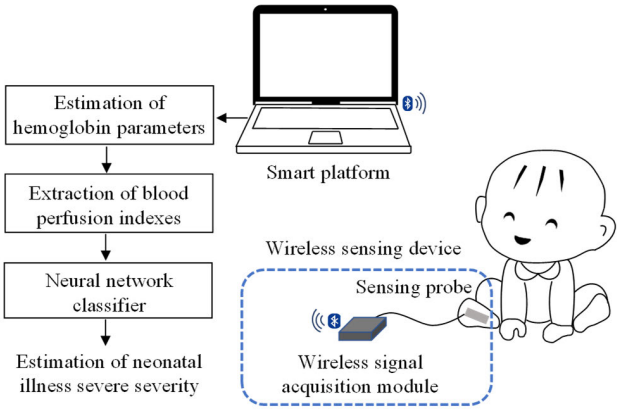

FIGURE 1. Schematic diagram of the proposed intelligent systemic circulation monitoring system.

The wireless sensing device contained a sensing probe and a wireless signal acquisition module, and its block diagram and photograph are shown in Fig. 2 (a) and Fig. 2 (b) respectively. The sensing probe, combining an optical sensor with a force sensor, was positioned on the bottom of the foot. The optical sensor contains a tri-wavelengths light-emitting diode (LED; SMT 640/700/910, Epitex, Tokyo, Japan) and a photodiode (PD; PD15-22/TR8, Everlight Electronics, Taipei, Taiwan), and they were used as the light source and light detector respectively. The distance between the light source and light detector was set to 10 mm. The force sensor (Flexiforce A301-1, Tekscan, Boston, MA, USA), that is a round flexible force sensing resistor, was used to detect the applied force on the skin. The wireless signal acquisition

module mainly consists of a microprocessor, a LED driver circuit, a photodiode amplifier circuit, a force sensing circuit, and a wireless communication circuit. The LED driver circuit was designed to control the LED turning on/ off via the microprocessor commands. When the LED was turned on to provide the light illumination on the human tissue, the light reflected from the human tissue would be received by the photodiode, and then would be converted into the electrical voltage signal and amplified by the photodiode amplifier circuit. In addition, the force sensor would detect the applied force externally on the skin surface of the foot sole, and then the force sensing circuit would convert the applied force signal into the voltage signal. Finally, these collected physiological signals would be digitized and sent to the wireless communication circuit by the microprocessor, to transmit to the smart platform wirelessly.

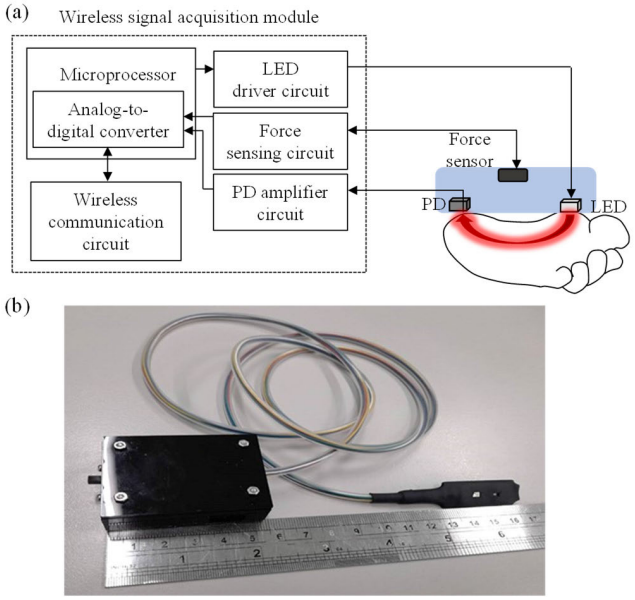

FIGURE 2. (a) Block diagram and (b) photograph of designed wireless sensing device.

B. ESTIMATION OF HEMOGLOBIN PARAMETERS

In the near-infrared wavelength (about 650 nm ∼ 950 nm), the light can provide the better penetrating depth for most human tissue components due to the relatively smaller absorbing and scattering properties. Because the transparency characteristic of the human tissue, the estimation of the major absorbers in the near-infrared light, such as oxy-hemoglobin (HbO_2) and deoxy-hemoglobin (Hb) [19] become possible. According to the distinctive absorbing and scattering properties, the hemoglobin concentration changes in human tissue can be simply estimated from the attenuation changes of dual or more wavelength near-infrared light. The modified Beer–Lambert law (MBLL) is the widely used algorithm to account the absorbing effect on light attenuation [20], [21].

The change of the optical density attenuation corresponding to the concentration change of the absorbing chromophore in the medium or human tissue components can be defined as the ratio of the light intensity after penetrating through the medium to the incident light intensity [22]. Therefore, in the irradiation of near-infrared light with human tissue, the change of the optical density attenuation $\Delta OD(\lambda)$ corresponding to the wavelength λ, caused by the hemoglobin concentration changes of $\Delta\,[HbO_2]$ and $\Delta[Hb]$, can be simply obtained as following [23].

$$\Delta OD(\lambda) = -log\frac{I_o\,(\lambda)}{I_i\,(\lambda)} = (\varepsilon^{\lambda}_{HbO_2}\cdot\Delta\,[HbO_2] + \varepsilon^{\lambda}_{Hb}\cdot\Delta[Hb])\cdot L\cdot B(\lambda) \tag{1}$$

Here, $I_o(\lambda)$ and $I_i(\lambda)$ represent the penetrating light intensity and the incident light intensity, and $\varepsilon^{\lambda}_{HbO_2}$ and $\varepsilon^{\lambda}_{Hb}$ are the extinction coefficients of HbO_2 and Hb respectively. The parameter L denotes the separation between the light source and the photodetector, and $B(\lambda)$ is the correcting factor for the photon progression pathway in human tissue [24]. From the above equation, the concentration changes of HbO_2 and Hb can then be estimated by the multi-wavelength optical density attenuations, as shown in followings [22], [25].

$$\Delta\,[HbO_2] = \frac{1}{\det(\mathrm{A})}\cdot\frac{1}{\mathrm{L}}\cdot\left(\varepsilon^{\lambda_2}_{Hb}\cdot\frac{\Delta OD\,(\lambda_1)}{\mathrm{B}(\lambda_1)} - \varepsilon^{\lambda_1}_{Hb}\cdot\frac{\Delta OD\,(\lambda_2)}{\mathrm{B}(\lambda_2)}\right) \tag{2}$$

$$\Delta[Hb] = \frac{1}{\det(\mathrm{A})}\cdot\frac{1}{\mathrm{L}}\cdot\left(\varepsilon^{\lambda_1}_{HbO_2}\cdot\frac{\Delta OD\,(\lambda_2)}{\mathrm{B}(\lambda_2)} - \varepsilon^{\lambda_2}_{HbO_2}\cdot\frac{\Delta OD\,(\lambda_1)}{\mathrm{B}(\lambda_1)}\right) \tag{3}$$

where $\det(\mathrm{A})$ is the determinant of a 2×2 matrix $\mathrm{A} = \begin{bmatrix} \varepsilon^{\lambda_1}_{HbO_2} & \varepsilon^{\lambda_1}_{Hb} \\ \varepsilon^{\lambda_2}_{HbO_2} & \varepsilon^{\lambda_2}_{HbO_2} \end{bmatrix}$. In this study, 700 nm and 910 nm wavelength lights were used because the absorption spectral coinciding point of HbO_2 and Hb is at about 800 nm. Finally, the changes of total hemoglobin (HbT) concentration and tissue oxygen saturation (StO_2) can then be estimated from the concentration changes of HbO_2 and Hb.

$$\Delta\,[HbT] = \Delta\,[HbO_2] + \Delta[Hb] \tag{4}$$

$$\Delta\,[StO_2] = \frac{\Delta\,[HbO_2]}{\Delta\,[HbO_2] + \Delta[Hb]}\cdot 100\% \tag{5}$$

C. EXTRACTION OF BLOOD PERFUSION INDEXES

In order to present the blood perfusion state, several indexes were defined from the change of the hemoglobin parameters (HbT and StO_2) under capillary refilling test, and they are illustrated in Fig. 3. The definition of Index I and VI is the initial HbT and StO_2 before applying the external pressure respectively, used to evaluate the baseline of blood circulation state. The definition of Index II and VII is the averaged HbT and StO_2 during the applied external pressure respectively. The definition of Index III and VIII is the averaged HbT and

StO_2 after releasing the applied pressure, used to evaluate the blood perfusion state. The definition of Index IV is the time amount of the HbT spent in reaching the highest level after pressure release, used to evaluate the capillary refilling time. The Index V is the difference of the capillary refilling time after the first pressure release and repeated pressure release.

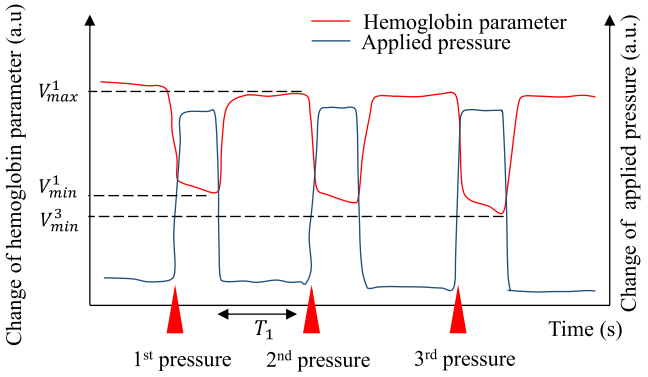

V^n_{min} : Min hemoglobin parameter after applying n-th pressure
V^n_{max} : Max hemoglobin parameter after releasing n-th pressure
T_n : Amount of time from HbT^n_{min} to HbT^n_{max}

Index I = Average of 2s HbT before 1st pressure
Index II = Average of 2s HbT before HbT^1_{min}
Index III = Average of 2s HbT before HbT^1_{max}
Index IV = T_1
Index V = Difference between T_1 and T_3
Index VI = Average of 2s StO_2before 1st pressure
Index VII = Average of 2s StO_2before $StO_2{}^1_{min}$
Index VIII = Average of 2s StO_2before $StO_2{}^1_{max}$

FIGURE 3. Illustration for defined indexes related to blood perfusion state.

D. NEURAL NETWORK CLASSIFIER FOR ESTIMATING NEONATAL ILLNESS SEVERE SEVERITY

In order to evaluate different illness severities from the blood perfusion state, the technique of radial basis function neural network (RBFNN) was used as a classifier in this study. RBFNN contains the advantages of simpler network structure, fast learning processing, and an excellent nonlinear approximation capability [26], and has been widely applied in many medical applications [27], [28], [29]. Its basic structure is a three-layer feedforward network (N_0 input neurons, N_1 hidden neurons, and one output neuron), as shown in Fig. 4. In this study, several indexes related to blood perfusion state and the hemoglobin concentration measured by the blood test, were used as the input of RBFNN. Here, the output of the j-th hidden neuron can be calculated by the Gaussian activation function [30],

$$\Phi_j(n) = \exp\left(-\frac{\|\boldsymbol{x}(n) - \boldsymbol{c_j}\|^2}{2\sigma^2}\right), \quad j = 1, 2, \ldots, N_1 \quad (6)$$

where $\boldsymbol{x}(n) = \left[x_1(n), x_2(n), x_3(n), \ldots, x_{N_0}(n)\right]^T$ denotes the input vector at the n-th trial, σ is the deviation of all input vectors, and $\boldsymbol{c_j}$ is the center vector of the j-th hidden neuron that can be viewed as the representative features extracted from the training data set via the unsupervised learning mode (k-mean clustering algorithm) [31]. The used Gaussian activation function can provide the nonlinear transform to evaluate the similarity between the center vector and the input vector, and can effectively enhance the nonlinear approximation capability of RBFNN [32]. Finally, the output of RBFNN is the linear combination of the outputs of all hidden neurons, and it can be expressed by

$$RBFNN\ output = \boldsymbol{\Phi}^{\boldsymbol{T}}(n) \cdot \boldsymbol{W} \quad (7)$$

where $\boldsymbol{\Phi}(n) = \left[\Phi_1(n), \Phi_2(n), \ldots, \Phi_{N_1}(n)\right]^T$ is the outputs of all hidden neurons, and $\boldsymbol{W} = \left[w_1, w_2, w_3, \ldots, w_{N_1}\right]^T$ is the weight vector between all hidden neurons and the output neuron. In this study, the normalized least mean square (NLMS) algorithm [33] was used to adjust the weight vector. According to Neonatal Therapeutic Intervention Scoring System (NTISS) the neonates with different illness severities were classified into two groups: the mild illness severity group (NTISS $\leq$ 15) and the severe illness severity group (NTISS $>$ 15). During the supervised learning processing, the desired output of RBFNN for the mild and severe illness groups were defined as 1 or 0 respectively.

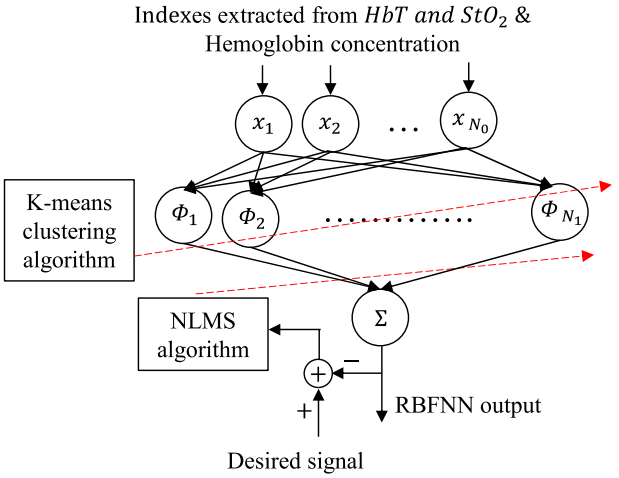

FIGURE 4. Architecture of radial basis function neural network.

E. EXPERIMENTAL DESIGN

In order to investigate the relationship between the blood perfusion state and the illness severity in neonates, the participating neonates were classified into two groups: the mild illness severity group (41 males and 21 females) and the severe illness severity group (11 males and 9 females). The averaged postnatal age of all neonates is 2.87 $\pm$ 2.14 days, and the information of these neonates are summarized in Table 1. In this experiment, the proposed sensing probe was placed on the bottom of the neonate foot. The healthcare worker would first apply a pressure on the sensing probe for 5 s, and then relaxed for 10 s. The above procedure would be repeated 3 times and each participating neonate would be measured for 6 times within one hour. This experiment has

been approved by the approval from the institutional review board of Kaohsiung Medical University Chung-Ho Memorial Hospital (IRB No. KMUHIRB-SV(I)-20200004), and the parents of all participated neonates have signed the informed consent form. The t-test was used to estimate the statistical significance, and the significance was defined as $p < 0.05$.

Moreover, the whole flowchart of signal processing is illustrated in Fig. 5. The change of hemoglobin parameters would first be estimated from multi-wavelength optical density attenuations, and then the defined indexes would be obtained. Next, the significant indexes would be selected as the input of classifier via several feature selection methods, including t-test, Kruskal-Wallis test, Relief, entropy-based information gain, entropy-based information gain ratio, entropy-based symmetrical uncertainty, one rule algorithm, and ranking based on mutual information. Finally, the optimal classifier would be determined from the performance of different classifiers, including decision tree (DT), K-nearest neighbors (KNN), logistic regression (LR), random forest (RF), support vector machine (SVM), and RBFNN.

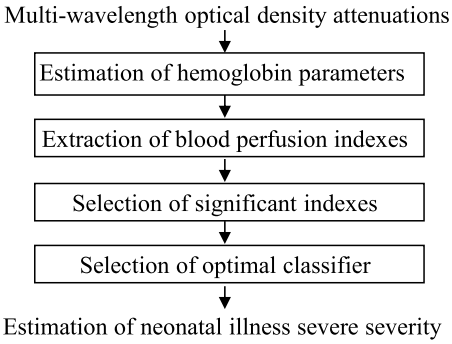

FIGURE 5. Whole flowchart of signal processing used in proposed system.

TABLE 1. Demographic data of measured neonates in different groups.

Group	Mild illness severity	Severe illness severity
Total No.	62	20
Male No.	41	11
Female No.	21	9
Postnatal age (days)	2.66 ± 2.07	3.50 ± 2.28
Gestational age (week)	34.98	30.60
Birth body weight (gm)	2349.52	1540.10
NTISS	≤ 15	> 15

III. EXPERIMENTAL RESULTS

A. NEONATAL BLOOD PERFUSION INDEXES CORRESPONDING TO DIFFERENT GROUPS

In this section, the blood perfusion indexes corresponding to different groups was first investigated. The experiment of results of Index I - VIII corresponding to different groups

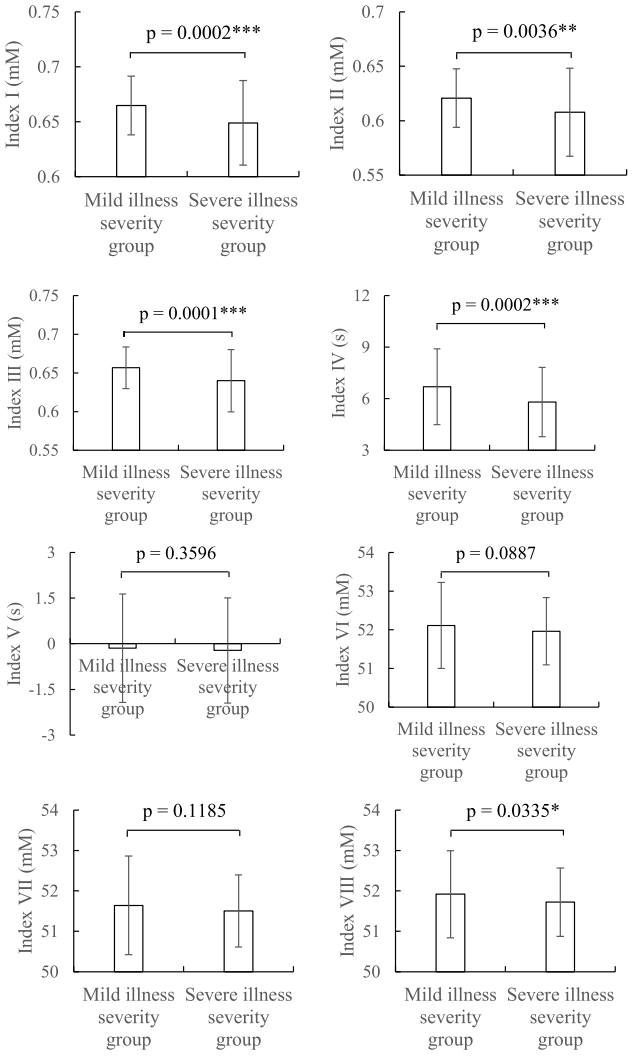

FIGURE 6. Experimental results of Index I-VIII corresponding to different groups (* $p < 0.05$, ** $p < 0.01$, *** $p < 0.001$).

TABLE 2. Experiment results of index I-VIII in different groups.

	Mild illness severity group	Severe illness severity group	*p*-value
Index I	0.665 ± 0.026	0.649 ± 0.039	0.0002
Index II	0.620 ± 0.026	0.607 ± 0.041	0.0036
Index III	0.657 ± 0.027	0.640 ± 0.040	0.0001
Index IV	6.700 ± 2.208	5.805 ± 2.010	0.0002
Index V	-0.144 ± 1.781	-0.219 ± 1.726	0.3596
Index VI	52.113 ± 1.111	51.962 ± 0.871	0.0887
Index VII	51.643 ± 1.218	51.505 ± 0.893	0.1185
Index VIII	51.919 ± 1.075	51.721 ± 0.842	0.0335

are shown in Fig. 6 and Table 2. From the experimental results, the Index I - III values of *HbT* concentration of the mild illness severity group were significantly higher than the severe illness severity group. The Index IV values of capillary refilling time of the mild illness severity group were significantly higher than the severe illness severity group. Here, the Index VIII values of StO_2 concentration of the mild illness

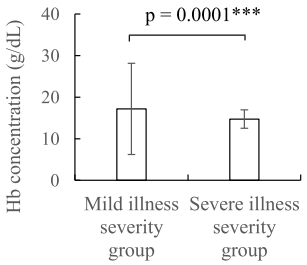

FIGURE 7. Hemoglobin concentration measured in blood corresponding to different groups (* $p < 0.05$, ** $p < 0.01$, *** $p < 0.001$).

severity group were also significantly higher than the severe illness severity group. Fig. 7 shows the hemoglobin concentration measured by the blood test corresponding to different groups. The experimental result showed a significant difference between the hemoglobin concentrations in the blood for the mild illness severity group (17.189 ± 10.949) and the severe illness severity group (14.722 ± 2.215, $p = 0.0001$).

B. NEONATAL BLOOD PERFUSION INDEXES CORRESPONDING TO DIFFERENT GROUPS

From the above experimental results, the difference between the Index I - IV, Index VIII and the hemoglobin concentration (Hb) in blood for different groups were significant. Therefore, in this study, the above self-defined Indexes and hemoglobin concentration in blood were used as the input of RBFNN to classify the illness severity. Here, a total 61 participants (48 mild illness severity cases and 13 severe illness severity cases) were randomly selected for training, and 21 participants (14 mild illness severity cases and 7 severe illness severity cases) were used for blind test. In order to optimize the classification performance of RBFNN, the threshold was set from 0 to 1, and the number of the hidden neurons was set to 16, 32, and 64. In addition to the hyperparameter test of the RBFNN classifier, we also perform hyperparameter tests for other common DT, KNN, LR, RF, and SVM classifiers, and all use the above 61 participants for hyperparameters finding. Tables 3 to 8 show the performance of each classifier in different hyperparameter ranges and combinations.

In order to evaluate the classification performance, several indicators for binary classification have to be defined. Here, true-positive (TP) and true-negative (TN) are correctly identify the mild illness severity group and the severe illness severity group respectively. False-positive (FP) means that the mild illness severity group is incorrectly identified as the severe illness severity group. False-negative (FN) is the severe illness severity group is incorrectly identified as the mild illness severity group. In this study, the classification performance was determined by the value of F-measure and accuracy, and they are defined as followings.

$$\text{Sensitivity} = \frac{TP}{TP + FN} \tag{8}$$

$$\text{Precision} = \frac{TP}{TP + FP} \tag{9}$$

$$\text{Specifcity} = \frac{TN}{TN + FP} \tag{10}$$

$$\text{Accuracy} = \frac{TP + TN}{TP + TN + FP + FN} \tag{11}$$

$$\text{F} - \text{measure} = 2 \cdot \frac{sensitivity \cdot precision}{sensitivity + precision} \tag{12}$$

The optimal hyperparameter combination of each model can be obtained from the above hyperparameter experiments, the results are shown in Table 9. The overall average performance can be seen that SVM and RBFNN have better performance, but they also have different advantages. Although all performance indicators of RBFNN are almost above the average, the low specificity still affects the AUC of the model, resulting in a low AUC. Although RBFNN still has some shortcomings, it is more energy-saving and time-saving than SVM, and the overall F-measure is also higher than SVM. Finally, we still choose RBFNN as the classifier of the proposed system. The results indicated that the RBFNN with 64 hidden neurons and threshold value of 0.6 could provide the better performance (F-measure = 92.36%, sensitivity = 95.04%, precision = 89.84%, specificity = 62.86%, and accuracy = 87.82%). For the blind test, the hidden neuron number and the given threshold were set to 64 and 0.6 respectively, and its classification performance was also good (F-measure = 90.27%, sensitivity = 90.27%, precision = 90.27%, specificity = 61.11%, and accuracy = 84.44%). The confusion matrix of the blind test is shown in Fig. 8.

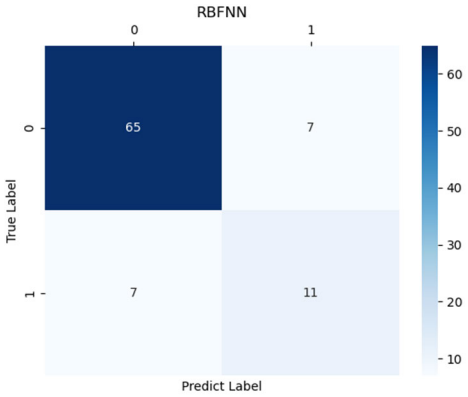

FIGURE 8. Confusion matrix of blind test result using RBFNN classifier.

In addition to the RBFNN classifier, we have selected five other common classifiers, including DT, KNN, LR, RF, and SVM classifiers, to test whether there will be better classification performance than RBFNN. We use indicators such as accuracy, sensitivity, precision, specificity, F-measure, and area under curve (AUC) to evaluate classifier performance. The comparison of classification performance of these six classifiers is shown in Table 10. After comparison, we take F -measure as the main comprehensive consideration, and we finally choose RBFNN as the classifier of this system.

Fig. 9 shows the RBFNN outputs for prediction illness severity in different groups. The mild illness severity group

TABLE 3. Performance comparison of DT classifier in different hyperparameter ranges and combinations.

Hyperparameter			Performance					
max_depth	class weight	criterion	Accuracy	Precision	Sensitivity	Specificity	F-measure	AUC
15			81.11	52.94	50	88.89	51.42	0.6944
12	0.25:1.5	gini	81.11	52.94	50	88.89	51.42	0.6944
9			78.89	47.36	50	86.11	48.64	0.6806
	0.2:1		76.67	41.18	38.89	86.11	40.00	0.625
15	0.2:1.5	gini	82.22	56.25	50	90.27	52.94	0.7014
	0.22:1.5		81.11	52.94	50	88.89	51.42	0.6944
	0.24:1.5		**83.33**	**60**	50	**91.67**	**54.55**	**0.7083**
15	0.24:1.5	entropy	74.44	40	**55.56**	79.17	46.51	0.6736

TABLE 4. Performance comparison of KNN classifier in different hyperparameter ranges and combinations.

Hyperparameter			Performance					
n_neighbors	weights	p	Accuracy	Precision	Sensitivity	Specificity	F-measure	AUC
		1	82.22	58.33	38.89	93.06	46.67	0.6597
5	uniform	2	80.00	50.00	33.33	91.67	40.00	0.625
		3	81.11	54.55	33.33	93.06	41.38	0.6319
5	distance	1	82.22	58.33	38.89	93.06	46.67	0.6597
3			82.22	58.33	38.89	93.06	46.67	0.6597
7	uniform	1	83.33	66.67	33.33	95.83	44.44	0.6458
9			86.67	87.50	38.89	98.61	53.85	0.6875
11			**87.78**	**88.89**	**44.44**	**98.61**	**59.26**	**0.7153**

TABLE 5. Performance comparison of LR classifier in different hyperparameter ranges and combinations.

Hyperparameter			Performance					
C	class_weight	n_jobs	Accuracy	Precision	Sensitivity	Specificity	F-measure	AUC
		1	80.00	50.00	61.11	84.72	55.00	0.7292
0.9	0.3:1.2	2	80.00	50.00	61.11	84.72	55.00	0.7292
		3	80.00	50.00	61.11	84.72	55.00	0.7292
0.7			80.00	50.00	61.11	84.72	55.00	0.7292
0.9	0.3:1.2	1	80.00	50.00	61.11	84.72	55.00	0.7292
1			81.11	52.38	61.11	86.11	**56.41**	0.7361
	0.3:1.0		**82.22**	**57.14**	44.44	**91.67**	50.00	0.6806
1	0.3:1.4	1	73.33	40.63	72.22	73.61	52.00	0.7292
	0.3:1.6		68.89	37.50	**83.33**	65.28	51.72	**0.7431**

TABLE 6. Performance comparison of RF classifier in different hyperparameter ranges and combinations.

Hyperparameter			Performance					
criterion	max_leaf_nodes	class_weight	Accuracy	Precision	Sensitivity	Specificity	F-measure	AUC
gini	none	0.25:2	87.78	88.89	44.44	98.61	59.26	0.7153
entropy			81.11	53.33	44.44	90.28	48.48	0.6736
	2		55.56	28.85	**83.33**	48.61	42.86	0.6597
gini	5	0.25:2	78.89	48.28	77.78	79.17	59.57	**0.7847**
	9		84.44	60.00	66.67	88.89	**63.16**	0.7778
	13		84.44	62.50	55.56	91.67	58.82	0.7361
gini	none	0.25:1.5	83.33	61.54	44.44	93.06	51.61	0.6875
		0.25:3	**88.89**	**100.00**	44.44	**100.00**	61.54	0.7222

TABLE 7. Performance comparison of SVM classifier in different hyperparameter ranges and combinations.

Hyperparameter			Performance					
kernel	class_weight	coef0	Accuracy	Precision	Sensitivity	Specificity	F-measure	AUC
poly	0.25:1.2	0.05	85.56	60.87	77.78	87.50	68.29	0.8264
rbf			75.56	44.12	83.33	73.61	57.69	0.7847
	0.27:1.2		90.00	73.68	77.78	93.06	75.68	0.8542
poly	0.29:1.3	0.05	92.22	82.35	77.78	95.83	80.00	0.8681
	0.30:1.2		**93.33**	**87.50**	**77.78**	**97.22**	**82.35**	**0.875**
		0.03	84.44	58.33	77.78	86.11	66.67	0.8194
poly	0.25:1.2	0.04	85.56	60.87	77.78	87.50	68.29	0.8264
		0.06	85.56	60.87	77.78	87.50	68.29	0.8264

(0.9335 ± 0.2356) was significantly higher than the severe illness severity group (0.5644 ± 0.2774, $p = 0.0000$) and the interventional treatment group (0.7628 ± 0.3039, $p = 0.0012$). The interventional treatment group was higher than the severe illness severity group ($p = 0.0130$). Here, the interventional therapy of the treatment group was evaluated

TABLE 8. Performance comparison of RBFNN classifier in different hyperparameter ranges and combinations.

Hyperparameter		Performance					
hidden neurons	threshold	Accuracy	Precision	Sensitivity	Specificity	F-measure	AUC
16	0.3	82.05	81.21	100	20	89.63	0.6
	0.4	83.65	82.59	100	27.14	90.47	0.6357
	0.5	83.97	83.57	98.76	32.86	90.53	0.6581
	0.6	82.69	83.81	96.28	35.71	89.62	0.66
32	0.3	82.37	81.69	99.59	22.86	89.76	0.6122
	0.4	84.62	84.64	97.93	38.57	90.80	0.6825
	0.5	84.29	86.42	94.63	48.57	90.34	0.716
	0.6	83.65	**90.99**	87.60	**70**	89.26	0.788
64	0.3	84.93	80.94	**100**	32.86	89.46	0.6643
	0.4	87.18	83.16	**100**	42.86	90.81	0.7143
	0.5	**88.78**	85.97	98.76	54.29	91.92	0.7652
	0.6	87.82	89.84	95.04	62.86	**92.36**	**0.7895**

TABLE 9. Optimal hyperparameter combination of each classifier.

Classifier	Hyperparameter
DT	max_depth=15 / class_weight=0.24:1.5 / criterion= gini
KNN	n_neighbors=11 / weights=uniform / p=1
LR	C=1 / class_weight=0.3:1 / n_jobs=1
RF	criterion=gini / max_leaf_nodes=none / class_weight=0.25:1.5
SVM	kernel=poly / class_weight=0.3:1.2 / coef0=0.05
RBFNN	Layers=64 / threshold=0.6

TABLE 10. Comparison of classification performance of six classifiers.

Classifier	Accuracy	Sensitivity	Precision	Specificity	F-measure	AUC
DT	81.11%	50.00%	52.94%	88.89%	51.43%	0.69
KNN	82.22%	38.89%	58.33%	93.06%	46.67%	0.66
LR	80.00%	61.11%	50.00%	84.72%	55.00%	0.73
RF	87.78%	44.44%	88.89%	98.61%	59.26%	0.72
SVM	85.56%	77.78%	60.87%	87.50%	68.29%	0.83
RBFNN	84.44%	90.27%	90.27%	61.11%	90.27%	0.76

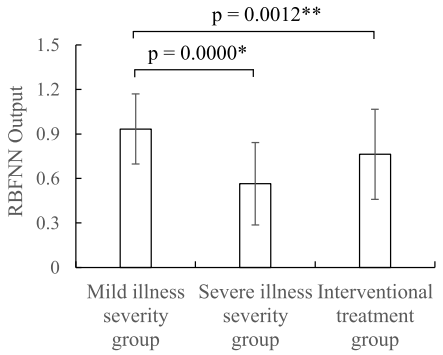

FIGURE 9. RBFNN outputs for prediction illness severity in different groups (* $p < 0.05$, ** $p < 0.01$, *** $p < 0.001$).

by the physician according to his/her clinical scenario and physician experience, and these infants have been treated with dopamine.

IV. DISCUSSIONS

From the experimental results, it indicates that the severe illness severity exactly reflected on several self-defined indexes. For the severe illness severity group, the lower Index I value of *HbT* might directly reflect the lower blood volume due to the lower vessel density or fewer hemoglobin concentration in the tissue of the infant under some disease states [34], [35]. In this study, some neonates in the severe illness severity group have patent ductus arteriosus (PDA), which leads to blood flowing from aorta to pulmonary artery resulting in a relative loss of systemic blood flow and pulmonary overloading [36]. Therefore, it might cause the relatively lower Index II value of *HbT* after applying pressure on the skin surface of the neonates with severe illness severity. The result of the Index III value of *HbT*, related to the capillary refill state after releasing the external pressure, was also lower in the severe illness severity group. Besides the influence of the difference between vessel densities of the mild and severe illness severity group, it might also be affected by the decrease of cardiac output and the systemic hypoperfusion. The Index IV was related to the amount of time spent by capillary refilling to the highest level after pressure release. For the mild illness severity group, the higher Index IV value of *HbT* might be resulted from its higher *HbT* level. Therefore, the capillary refill time in mild illness severity group was relatively longer than the severe illness severity group. Index VI – VIII were related to the changes of StO_2 at blood perfusion state caused by various pressure levels respectively. From the results of Index VI and VII, the

TABLE 11. Comparison between proposed system and other systems.

	LDF [37]	OPS imaging [39]	MRI [42]	Proposed system
Measurement technique	Doppler frequency shift	Polarization light technology	Nuclear magnetic resonance	Near-infrared spectroscopy
Wavelength of light source	780 nm	548 nm	-	700, 910 nm
Handheld device	No	Yes	No	Yes
Parameters	Blood flow velocity	2-D images	3-D images	Hemoglobin parameters
Classifier	-	-	-	RBFNN
Applications	Estimation of microcirculatory blood flow velocity	Estimation of the sublingual microcirculation	Assessment of microvascular dysfunction in organs	Estimation of peripheral blood perfusion
Advantages	Higher time resolution	Visualization of microvascular structure and distribution	Visualization of vascular structure and distribution, excellent soft-tissue contrast in organs	Non-invasive measurement, and real time estimation of blood perfusion, and NTISS
Limitations	Influence of motion artifacts, and lower spatial resolution and reproducibility	Influence of motion artifacts, and time-consuming analysis	Requirement of sedation or anesthesia for neonates, and expensive and nonportable equipment	Lack of detail blood vessel spatial information

differences between mild and severe illness severity group were insignificant, and this may be due to that the effect of vascular occlusion state caused by the short-term applied pressure on the oxygen consumption was still unobvious. However, the Index VIII related to the capillary refill state after the pressure release, for the severe illness severity group was relatively lower, and this may be due to the poorer fresh blood perfusion ability in the severe illness severity group.

Regarding to choose the classifier, the performance differences of each classifier shown in Table 10 are obvious, which may be caused by the different characteristics of each classifier. Classifiers such as DT/RF/ANN/LR use linear algorithms to distinguish mild from severe. This method may cause data that is too close to the midline to be classified into the wrong area by the classifier. And because the data of mild and severe are based on NTISS$<=$15 and $>$15. Therefore, when the amount of data in this study is insufficient and KNN is used as the classifier, data with NTISS around 15 may be easily misjudged. SVM maps data into a high-dimensional feature space and uses hyperplanes to classify the data. The RBFNN used in this study also uses a nonlinear algorithm to randomly focus on several feature points and calculate the information content. In this study, It is not easy to collect newborns with systemic circulatory disorders, especially critically ill newborns. Although the data is still insufficient, the AUCs after simply running various classifiers are all greater than 0.5, which means that the data extracted in this study still has predictive value.

Several approaches, related to estimate the blood circulation in clinical, have been proposed in the previous studies, and the comparison between these approaches and the proposed system is summarized in Table 11. LDF is a high-temporal-resolution technique for estimation of microcirculatory blood flow velocity. But, LDF cannot provide the deeper tissue blood perfusion assessment due to the poor spatial resolution, limited to the volume of 1 mm^3 and the penetration depth of about 1 mm. The large spatial information variability also results in the poor reproducibility [37], [38]. The OPS imaging can be utilized for high-resolution imaging of microvasculature and visualization of vessel structure and distribution [39]. But this approach suffers from the longer scanning duration, and the offline post-image processing is also time-consuming [40]. Additionally, high blood velocity cannot be measured since the OPS results are susceptibility to pressure and movement artifacts, which will induce image blurring and suboptimal imaging of the capillaries [41]. MRI can provide the visualization of vascular structure and excellent soft-tissue contrast in organs [42]. However, it requires the high magnetic field to operate, and moreover, the prolonged acquisition time leads to motion artifacts to cause a detrimental impact on image quality. The requirement of the expensive cost and the experienced operator also limits the clinical applicability [43], [44]. Although the above approaches can provide the information of blood flow rate and vascular distribution in the local tissue, but they cannot estimate the systemic circulation directly and further evaluate neonatal illness severe severity. Based on the NIRS technique, the proposed system could non-invasively access the change of hemoglobin parameters under the repeated pressure to estimate the state of blood perfusion. Moreover, by combining with the neural network technique, the mild and severe NTISS could also be successfully recognized. Furthermore, the proposed system contains the advantages of lower cost, easy operation, and non-invasive and real-time measurement. Despite the lack of precise blood vessel spatial information, the proposed system may provide the great potential in the clinical application of evaluating the systemic circulation and the effectiveness of interventional therapy for neonates in the future.

V. CONCLUSION

An intelligent systemic circulation monitoring system was successfully designed and implemented in this study. Based on the NIRS technique, the proposed system real-time and non-invasively accessed the changes of $\boldsymbol{HbT}$ and $\boldsymbol{StO_2}$ simultaneously under applied and released pressure, and several indexes related to the blood perfusion were further calculated from the change of hemodynamic response. The preliminary experimental results in a clinical setting indicated these defined indexes exactly contained the significant relationship between the mild and severe illness severity groups. For the severe illness severity group, the total hemoglobin concentration in the tissue under the applied pressure and tissue oxygen saturation after releasing the pressure were significantly lower, which were more likely to reflect low blood volume and systemic hypoperfusion. But the capillary refill time after releasing the external pressure in the mild severe severity group was relatively longer. Furthermore, by utilizing the neural network as classifier, the proposed system could successfully distinguish different groups from these defined indexes. The proposed system contains the advantages of non-invasive and real-time measurement, simple operation and lower cost. Therefore, the proposed system contains the potential of supplementary diagnostic tool for the future clinical application, assisting physicians to indirectly monitor the effects of treatment on the neonatal systemic circulation, and further predict mild and severe illness severity. Moreover, in the future, it also could combine with ECG measurement, and the heart rate and its variability might be useful and could serve as a comprehensive setup.

REFERENCES

[1] P.-L. Wu, W.-T. Lee, P.-L. Lee, and H.-L. Chen, "Predictive power of serial neonatal therapeutic intervention scoring system scores for short-term mortality in very-low-birth-weight infants," *Pediatrics Neonatology*, vol. 56, no. 2, pp. 108–113, Apr. 2015.

[2] B. Garg, D. Sharma, and N. Farahbakhsh, "Advanced hemodynamic monitoring in the neonatal intensive care unit," *J. Matern.-Fetal Neonatal Med.*, vol. 31, no. 10, pp. 1373–1380, Apr. 2017.

[3] W.-P. de Boode, "Advanced hemodynamic monitoring in the neonatal intensive care unit," *Clinics Perinatology*, vol. 47, no. 3, pp. 423–434, Sep. 2020.

[4] J. Sevransky, "Clinical assessment of hemodynamically unstable patients," *Current Opinion Crit. Care*, vol. 15, no. 3, pp. 234–238, Jun. 2009.

[5] W.-P. de Boode, "Clinical monitoring of systemic hemodynamics in critically ill newborns," *Early Hum. Develop.*, vol. 86, no. 3, pp. 137–141, Mar. 2010.

[6] K. Shinozaki, L. S. Jacobson, K. Saeki, H. Hirahara, N. Kobayashi, S. Weisner, J. M. Falotico, T. Li, J. Kim, and L. B. Becker, "Comparison of point-of-care peripheral perfusion assessment using pulse oximetry sensor with manual capillary refill time: Clinical pilot study in the emergency department," *J. Intensive Care*, vol. 7, no. 1, pp. 1–9, Dec. 2019.

[7] G. A. Holloway and D. W. Watkins, "Laser Doppler measurement of cutaneous blood flow," *J. Investigative Dermatol.*, vol. 69, no. 3, pp. 306–309, Sep. 1977.

[8] D. A. Low, H. Jones, N. T. Cable, L. M. Alexander, and W. L. Kenney, "Historical reviews of the assessment of human cardiovascular function: Interrogation and understanding of the control of skin blood flow," *Eur. J. Appl. Physiol.*, vol. 120, no. 1, pp. 1–16, Nov. 2019.

[9] S. Gupta and S. M. Donn, "Assessment of neonatal perfusion," *Seminars Fetal Neonatal. Med.*, vol. 25, no. 5, Oct. 2020, Art. no. 101144.

[10] B. K. Han, D. M. Overman, K. Grant, K. Rosenthal, S. Rutten-Ramos, D. Cook, and J. R. Lesser, "Non-sedated, free breathing cardiac CT for evaluation of complex congenital heart disease in neonates," *J. Cardiovascular Comput. Tomogr.*, vol. 7, no. 6, pp. 354–360, Nov. 2013.

[11] W. Groner, J. W. Winkelman, A. G. Harris, C. Ince, G. J. Bouma, K. Messmer, and R. G. Nadeau, "Orthogonal polarization spectral imaging: A new method for study of the microcirculation," *Nature Med.*, vol. 5, no. 10, pp. 1209–1212, Oct. 1999.

[12] R. Boushel, H. Langberg, J. Olesen, J. Gonzales-Alonzo, J. Bülow, and M. Kjaer, "Monitoring tissue oxygen availability with near infrared spectroscopy (NIRS) in health and disease," *Scandin. J. Med. Sci. Sports*, vol. 11, no. 4, pp. 213–222, Dec. 2001.

[13] F. Harel, A. Denault, Q. Ngo, J. Dupuis, and P. Khairy, "Near-infrared spectroscopy to monitor peripheral blood flow perfusion," *J. Clin. Monitor. Comput.*, vol. 22, no. 1, pp. 37–43, Nov. 2007.

[14] S. J. Thomson, M. L. Cowan, D. M. Forton, S. J. Clark, S. Musa, M. Grounds, and T. M. Rahman, "A study of muscle tissue oxygenation and peripheral microcirculatory dysfunction in cirrhosis using near infrared spectroscopy," *Liver Int.*, vol. 30, no. 3, pp. 463–471, Mar. 2010.

[15] J. E. Varela, S. M. Cohn, G. D. Giannotti, M. O. Dolich, H. Ramon, J. A. Wiseberg, and M. McKenney, "Near-infrared spectroscopy reflects changes in mesenteric and systemic perfusion during abdominal compartment syndrome," *Surgery*, vol. 129, no. 3, pp. 363–370, Mar. 2001.

[16] S. A. H. Shah, A. di Terlizzi, and M. A. Deriu, "Intelligent system development to monitor the neonatal behaviour: A review," in *Proc. CEUR Workshop*, Ljubljana, Slovenia, Aug. 2022, pp. 133–146.

[17] S. Mishra, G. A. Khouqeer, B. Aamna, A. Alodhayb, S. J. Ali Ibrahim, M. Hooda, and G. Jayaswal, "A review: Recent advancements in sensor technology for non-invasive neonatal health monitoring," *Biosensors Bioelectronics, X*, vol. 14, Sep. 2023, Art. no. 100332.

[18] A. A. Chakkarapani, C. C. Roehr, S. B. Hooper, A. B. T. Pas, and S. Gupta, "Transitional circulation and hemodynamic monitoring in newborn infants," *Pediatric Res.*, pp. 1–9, 2023, doi: 10.1038/S41390-022-02427-8.

[19] G. Strangman, D. A. Boas, and J. P. Sutton, "Non-invasive neuroimaging using near-infrared light," *Biol. Psychiatry*, vol. 52, no. 7, pp. 679–693, Oct. 2002.

[20] W. B. Baker, A. B. Parthasarathy, D. R. Busch, R. C. Mesquita, J. H. Greenberg, and A. G. Yodh, "Modified Beer-Lambert law for blood flow," *Biomed. Opt. Exp.*, vol. 5, no. 11, pp. 4053–4075, 2014.

[21] J.-R. Kuo, B.-S. Lin, C.-L. Cheng, and C.-C. Chio, "Hypoxic-state estimation of brain cells by using wireless near-infrared spectroscopy," *IEEE J. Biomed. Health Informat.*, vol. 18, no. 1, pp. 167–173, Jan. 2014.

[22] K.-D. Lin, B.-S. Lin, G.-A. Lin, and B.-S. Lin, "Design of smart peripheral blood perfusion monitoring system for diabetics," *IEEE Sensors J.*, vol. 21, no. 8, pp. 10167–10173, Apr. 2021.

[23] Y.-K. Huang, C.-C. Chang, P.-X. Lin, and B.-S. Lin, "Quantitative evaluation of rehabilitation effect on peripheral circulation of diabetic foot," *IEEE J. Biomed. Health Informat.*, vol. 22, no. 4, pp. 1019–1025, Jul. 2018.

[24] D. A. Boas, T. Gaudette, G. Strangman, X. Cheng, J. J. A. Marota, and J. B. Mandeville, "The accuracy of near infrared spectroscopy and imaging during focal changes in cerebral hemodynamics," *NeuroImage*, vol. 13, no. 1, pp. 76–90, Jan. 2001.

[25] W. Chou, P.-J. Wu, C.-C. Fang, Y.-S. Yen, and B.-S. Lin, "Design of smart brain oxygenation monitoring system for estimating cardiovascular disease severity," *IEEE Access*, vol. 8, pp. 98422–98429, 2020.

[26] H. Han, Q. Chen, and J. Qiao, "Research on an online self-organizing radial basis function neural network," *Neural Comput. Appl.*, vol. 19, no. 5, pp. 667–676, Jul. 2010.

[27] B.-S. Lin, M.-J. Sheu, C.-C. Chuang, K.-C. Tseng, and J.-Y. Chen, "Enhancing bowel sounds by using a higher order statistics-based radial basis function network," *IEEE J. Biomed. Health Informat.*, vol. 17, no. 3, pp. 675–680, May 2013.

[28] B.-S. Lin, B.-S. Lin, F.-C. Chong, and F. Lai, "Higher order statistics-based radial basis function network for evoked potentials," *IEEE Trans. Biomed. Eng.*, vol. 56, no. 1, pp. 93–100, Jan. 2009.

[29] H.-Y. Wang, C.-H. Wu, C.-Y. Chen, and B.-S. Lin, "Novel noninvasive approach for detecting arteriovenous fistula stenosis," *IEEE Trans. Biomed. Eng.*, vol. 61, no. 6, pp. 1851–1857, Jun. 2014.

[30] B.-S. Lin, B.-S. Lin, F.-C. Chong, and F. Lai, "Higher-order-statistics-based radial basis function networks for signal enhancement," *IEEE Trans. Neural Netw.*, vol. 18, no. 3, pp. 823–832, May 2007.

[31] R. Rollet, G. B. Benie, W. Li, S. Wang, and J.-M. Boucher, "Image classification algorithm based on the RBF neural network and K-means," *Int. J. Remote Sens.*, vol. 19, no. 15, pp. 3003–3009, Jan. 1998.
[32] S. Yang, T. O. Ting, K. L. Man, and S. U. Guan, "Investigation of neural networks for function approximation," *Proc. Comput. Sci.*, vol. 17, pp. 586–594, Jan. 2013.
[33] P. E. An, B. Brown, and C. J. Harris, "On the convergence rate performance of the normalized least-mean-square adaptation," *IEEE Trans. Neural Netw.*, vol. 8, no. 5, pp. 1211–1214, Sep. 1997.
[34] J. Jopling, E. Henry, S. E. Wiedmeier, and R. D. Christensen, "Reference ranges for hematocrit and blood hemoglobin concentration during the neonatal period: Data from a multihospital health care system," *Pediatrics*, vol. 123, no. 2, pp. e333–e337, Feb. 2009.
[35] D. De Backer and A. Durand, "Monitoring the microcirculation in critically ill patients," *Best Pract. Res. Clin. Anaesthesiology*, vol. 28, no. 4, pp. 441–451, Dec. 2014.
[36] N. Evans, "Patent ductus arteriosus in the neonate," *Current Paediatrics*, vol. 15, no. 5, pp. 381–389, Oct. 2005.
[37] Y. A. Abdulhameed, G. Lancaster, P. V. McClintock, and A. Stefanovska, "On the suitability of laser-Doppler flowmetry for capturing microvascular blood flow dynamics from darkly pigmented skin," *Physiol. Meas.*, vol. 40, no. 7, Jul. 2019, Art. no. 074005.
[38] A. Humeau-Heurtier, E. Guerreschi, P. Abraham, and G. Mahé, "Relevance of laser Doppler and laser speckle techniques for assessing vascular function: State of the art and future trends," *IEEE Trans. Biomed. Eng.*, vol. 60, no. 3, pp. 659–666, Mar. 2013.
[39] R. van Zijderveld, C. Ince, and R. O. Schlingemann, "Orthogonal polarization spectral imaging of conjunctival microcirculation," *Graefe's Arch. Clin. Experim. Ophthalmol.*, vol. 252, no. 5, pp. 773–779, Mar. 2014.
[40] J. Neubauer-Geryk, M. Hoffmann, M. Wielicka, K. Piec, G. Kozera, and L. Bieniaszewski, "Current methods for the assessment of skin microcirculation: Part 2," *Adv. Dermatol. Allergol.*, vol. 36, no. 4, pp. 377–381, 2019.
[41] C. Sturesson, J. Nilsson, and S. Eriksson, "Non-invasive imaging of microcirculation: A technology review," *Med. Devices, Evidence Res.*, vol. 7, pp. 445–452, Dec. 2014.
[42] M. C. Liszewski, P. Ciet, and E. Y. Lee, "MR imaging of lungs and airways in children: Past and present," *Magn. Reson. Imag. Clinics North Amer.*, vol. 27, no. 2, pp. 201–225, May 2019.
[43] R. C. Mathew and C. M. Kramer, "Recent advances in magnetic resonance imaging for peripheral artery disease," *Vascular Med.*, vol. 23, no. 2, pp. 143–152, Apr. 2018.
[44] J. Silickas, S. A. Black, A. Phinikaridou, A. M. Gwozdz, A. Smith, and P. Saha, "Use of computed tomography and magnetic resonance imaging in central venous disease," *Methodist DeBakey Cardiovascular J.*, vol. 14, no. 3, pp. 188–195, 2018.

HSIU-LIN CHEN received the M.D. degree from the Kaohsiung Medical College, Kaohsiung, Taiwan, in 1995, and the Master of Medical Science degree from the Graduate Institute of Medicine, Kaohsiung Medical University, in 2007. She is currently an attending Physician with the Division of Neonatology, Department of Pediatrics, Kaohsiung Medical University Hospital, and a Professor with the Department of Respiratory Therapy, School of Medicine, Kaohsiung Medical University. Her research interests include neonatal intensive care and management of premature infants.

BOR-SHING LIN (Senior Member, IEEE) received the B.S. degree in electrical engineering from National Cheng Kung University, Taiwan, in 1997, and the M.S. and Ph.D. degrees in electrical engineering from National Taiwan University, Taiwan, in 1999 and 2006, respectively. He is currently a Distinguished Professor with the Department of Computer Science and Information Engineering, and the Director of the Computer Center, National Taipei University, Taiwan. His research interests include smart medicine, embedded systems, wearable systems, biomedical signal processing, biomedical image processing, and portable biomedical electronic system design. He is a fellow of the Institution of Engineering and Technology (IET), U.K., and the British Computer Society (BCS), U.K.

KAI-HUEI CHEN received the M.S. degree from the Institute of Imaging and Biomedical Photonics, National Yang Ming Chiao Tung University, Taiwan. Her research interests include biomedical circuits and systems, biomedical signal processing, and biomedical optoelectronics.

BOR-SHYH LIN (Senior Member, IEEE) received the B.S. degree from National Chiao Tung University, Hsinchu, Taiwan, in 1997, and the M.S. and Ph.D. degrees from the Institute of Electrical Engineering, National Taiwan University, Taipei, Taiwan, in 1999 and 2006, respectively. He is currently a Distinguished Professor and the Director of the Institute of Imaging and Biomedical Photonics, National Yang Ming Chiao Tung University. He is a fellow of the Institution of Engineering and Technology (IET), U.K. His current research interests include biomedical circuits and systems, biomedical signal processing, and biosensor.